Science Arts & Métiers (SAM)
is an open access repository that collects the work of Arts et Métiers Institute of Technology researchers and makes it freely available over the web where possible.

This is an author-deposited version published in: https://sam.ensam.eu
Handle ID: .http://hdl.handle.net/10985/17726

To cite this version :

Sid-Ali AMAMRA, Frédéric COLAS, Xavier GUILLAUD, Pierre RAULT, Samuel NGUEFEU - Laboratory Demonstration of a Multiterminal VSC-HVDC Power Grid - IEEE Transactions on Power Delivery - Vol. 32, n°5, p.2339-2349 - 2017

Any correspondence concerning this service should be sent to the repository Administrator : scienceouverte@ensam.eu

Laboratory Demonstration of a Multi-Terminal VSC-HVDC Power Grid

Sid-Ali AMAMRA, Frederic COLAS, Xavier GUILLAUD, *Member, IEEE,* Pierre RAULT and Samuel NGUEFEU, *Member, IEEE,*.

***Abstract*—This paper presents the design, development, control and supervision of a hardware-based laboratory Multi-Terminal-Direct-Current (MTDC) test-bed. This work is a part of the TWENTIES (Transmission system operation with large penetration of Wind and other renewable Electricity sources in Networks by means of innovative Tools and Integrated Energy Solutions) DEMO 3 European project which aims to demonstrate the feasibility of a DC grid through experimental tests. This is a hardware-in-the-loop DC system test-bed with simulated AC systems in real time simulation; the DC cables and some converters are actual, at laboratory scale. The laboratory scale test-bed is homothetic to a full scale high voltage direct current (HVDC) system: electrical elements are the same in per unit. The test-bed is supervised by a Supervisory Control And Data Acquisition (SCADA) system based on PcVue. Primary control based droop control method to provide DC grid power balance and coordinated control methods to dispatch power as scheduled by transmission system operator (TSO) are implemented. Since primary control acts as converter level by using local measurements, a coordinated control is proposed to manage the DC grid power flow. The implemented system is innovative and achievable for real-time, real-world MTDC-HVDC grid applications.**

***Index Terms*—High Voltage Direct Current, Multi-Terminal DC, AC-DC grid Interactions, SCADA Supervision, Hardware In the Loop, Voltage Source Converter , Droop control, Coordinated control, DC Load-Flow, AC congestion, station outage.**

I. Introduction

EUROPEAN energy policy requires both an increase of renewable production in the energy mix and the reduction of CO2 emissions. Integrating more wind energy in the European power system is one answer to these objectives. As new onshore sites tend to be increasingly scarce due to a reduction of potential physical space [1], [2], there is a growing interest in locating wind farms off-shore. This has made manufacturers go beyond the boundaries imposed by onshore installations and reach toward offshore challenges[3]. The use of DC transmissions to connect offshore production far from the coast ($i.e.$ with better energy production potential) is mandatory. Historically, the main reason which led to the development of the DC technology was the transmission efficiency over long distances in terms of losses, compared with a corresponding AC transmission system, owing to no reactive power transport [4]. The willingness to integrate offshore wind farms and the improvement of DC to AC high power conversion tend to increase the field of application for DC transmissions [5]. Regarding offshore wind farms, most of the planned DC transmission systems are currently point-to-point links [6]. To achieve viability and, increase flexibility and reliability, a possible evolution would be to interconnect and even mesh the point-to-point links to finally obtain Multi-Terminal Direct Current (MTDC) systems [7], [8]. In fact, aggregating the wind power into a MTDC system contributes to balancing the regional wind power fluctuation, because the cross correlation of wind speeds in various geographical locations is much lower than within the same region [9]. However, the development of MTDC grids is a real breakthrough and remains an important technological challenge especially in terms of meshed grid. Lots of publications have already been written on these topics [10], [11], [12], and the results are mainly based on offline simulations since the development of a Multi MW demonstrator is very expensive or does not include real cables. An intermediate stage, which is proposed in this paper, is to develop a small scale actual MTDC interacting with a real time simulated AC system using a Power Hardware In the Loop (PHIL) simulation [13]. This concept makes it possible to test, with cost effectiveness, the behavior of actual devices in nearly real situations. The mock-up presented in this paper uses this PHIL principle and consists of a five-station DC network, which connects three off-shore wind farms to two on-shore terminals. Since the power electronic converters are considered as very scalable, this kind of mock-up provides the ability to validate control algorithms devoted to DC grids in a very realistic environment. As it is based on a PHIL simulation, this mock-up has been designed to test different kinds of control strategies, to assess the initialization and termination process. It is also possible to consider a communication link between stations and a SCADA system, and the topology of the grid is totally reconfigurable. Different types of experimentation may be imagined on this equipment; this paper is focused on power flow control, while the protection scheme has been dealt with in [14]. Different control schemes of the MTDC power grid have been proposed such as in [15]. In this paper, a hierarchical control strategy inspirited from an AC power system [16] has been implemented and tested. It is based on two levels: a local control level and a remote control level. In the local level, droop controllers have been used [17]. It has been demonstrated [18] that the voltage response time depends

This work is part of the TWENTIES Demo3 European project and has been funded by the 7th Framework Program (FP7) of the European Commission http://www.twenties-project.eu. It was supported financially by Réseaux de Transport Electrique - France. http://www.rte-france.com.

Sid-Ali AMAMRA, Frédéric COLAS and Xavier GUILLAUD are with Univ. Lille, Centrale Lille, Arts et Metiers Paristech, HEI, EA 2697 – L2EP, Laboratoire d'Electrotechnique et d'Electronique de Puissance, F-59000 Lille, France (Email: sidali.amamra@yncrea.fr)

Pierre RAULT and Samuel Nguefeu are with RTE National Centre for Grid Expertise Paris, France

on the converter station capacitors ($i.e.$ electrostatic constant), on the droop parameter k and on the number of stations which control the DC voltage m. A novel methodology to design the droop parameter is presented. It is based on voltage control loop response time and final voltage deviation choices, and takes into account the number of substations which participate, or not, in the voltage control. However, the main weakness of droop control is that power-flow dispatch is not perfectly controlled. A remote control level is then mandatory to improve power-flow dispatch. A master controller based on coordinated control with a modified Newton-Raphson load flow algorithm has been implemented for that. Following the system operator's orders and the scheduled power transmissions, the master controller sends references to all DC grid devices. It takes into account the voltage drops and transmission losses to send suitable converter settings in order to achieve a precise power flow control. It can also communicate with the TSO of the connected AC grid to alleviate AC congestion. The Numerical method to calculate steady state operating points to find suitable set points for DC grid devices is presented. The main contributions of this paper are: - Firstly: The development of a laboratory scale five-station/five-line MTDC grid to reflect at best the expected behavior of a future HVDC grid, to provide enough flexibility to test different DC and AC network topologies and to compare different control laws based on actual DC cables. - Secondly: The development and integration of a real-time control and supervision system based on an association of a local and a remote control level. The remainder of this paper is organized as follows: The proposed DC system configuration and modeling is provided in section II. Section III describes the proposed local and master controllers of the MTDC grid. Conclusions are summarized in Section IV.

II. CONFIGURATION AND MODELING OF THE PROPOSED SYSTEM

An overview of the five-terminal DC grid test-bed is presented in Fig. 1.

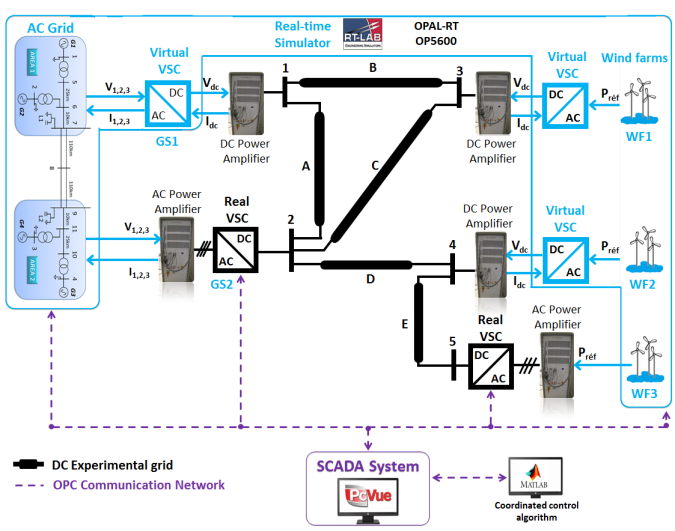

Fig. 1. Test-bed general overview

The test-bed is divided in two main parts; one physical part in the center of the figure in black and one virtual part simulated and implemented in Opal-RT® real-time simulator in blue. The interface between physical devices and the real time simulator analog outputs with two solutions:

- Actual two-level VSC connected to the real time simulator with three-phased AC power amplifier
- Virtual two-level VSC connected to the DC grid with DC power amplifier

The grid is composed of low voltage DC cables composed of two symmetrical poles. The AC grid, wind farms and virtual VSCs are simulated in the real-time simulator. Finally, the DC system is monitored and controlled by a SCADA system called PcVue, which receives information from VSCs or the real-time simulator and then sends set points to them thanks to an OPC communication protocol.

A. Laboratory scale of HVDC grid

To better reflect the behavior of a high voltage DC grid, special attention was paid during the design process to have a homothetic design of the major components constituting the DC grid.

1) Converter station design and control: Converter stations used in the test-bed are classical 2-level converters associated with an LCL filter for mitigating the current harmonics on the AC side, and a DC capacitor and smoothing reactors on the DC side Fig. 2.

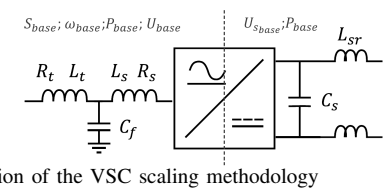

Fig. 2. Validation of the VSC scaling methodology

The equivalence between high power converter and the test-bed converter can be easily achieved thanks to the per unit transformation. It has been demonstrated that energy stored in the DC system characterizes its dynamics. AC system dynamics are characterized by the kinetic energy stored in synchronous rotating machines connected to it. For DC systems, the energy is stored in an electrostatic form since it corresponds mainly to the energy stored in converter station capacitors; this stored energy could be expressed by:

$$E_C = \frac{1}{2} C_S u_S^2 \tag{1}$$

Where:

u_S	is the DC voltage [V]
C_S	is the converter station capacitor [F]
E_S	is the energy stored in a converter station capacitor [J]

The same approach can be applied for the smoothing reactor design:

$$E_L = \frac{1}{2} L_S I_{base}^2 \tag{2}$$

TABLE I
PER UNIT APPROACH FOR CONVERTER STATION DESIGN

	Parameters	High power converter	Per unit	Test-bed converter
AC side	S_{base}	1077MVA	1 p.u.	3 kVA
	U_{base}	230kV	1 p.u.	125 V
	LCL cut-off frequency	500Hz	-	1 kHz
	R_S	0.48Ω	0.005 p.u.	0.026 Ω
	L_S	45mH	0.15 p.u.	2.5 mH
	R_t	0.48Ω	0.005 p.u.	0.026 Ω
	L_t	45mH	0.15 p.u.	2.5 mH
	C_f	4.47μF	-	20.4 μF
DC side	$U_{s\,base}$	640kV	1 p.u.	250 V
	P_{base}	1000MW	1 p.u.	2.5 kW
	C_s	50μF	10.24 ms	819 μF
	L_{SR}	10mH	1.10^{-2} ms	610 mH

Where:

I_{base} is the AC current [A]

L_S is the converter station inductance [H]

E_L is the energy stored in a converter station inductor [J]

Physical converter stations on the mock-up are rated at 3 kVA /125 V- 2.5 kW / 250 V. Their design is based on data from a 1077 MVA - 1000 MW converter station [2]. Passive component values are summarized in Table I. Fig. 3 A,B and C show three types of power-voltage control strategies for the VSC, *i.e.* characteristics implemented to control VSC (constant power, constant voltage or droop control). In order to validate the scaling methodology, the same simple off-line simulation is carried out for the high and low voltage converters.

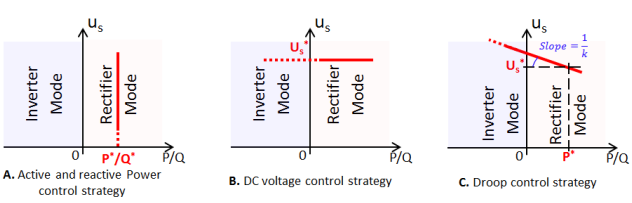

Fig. 3. VSC control strategy

Fig. 4 shows, in per unit, the comparison results from the low-voltage converter and from its high voltage. Power and voltage curves from the simulation of each converter are very similar; therefore the scaling methodology is validated. Two physical two-level VSCs based on the aforementioned methodology have been developed. It is based on the IGBT module [19]. The low level control has been implemented on a DSP card [19]. The gateway with the SCADA system is ensured by a Beckhoff PLC.

2) DC cable design and modeling: The DC cable should ensure wave propagation, hence it is not possible to emulate the DC cable by a simple RLC circuit, such as Π equivalent

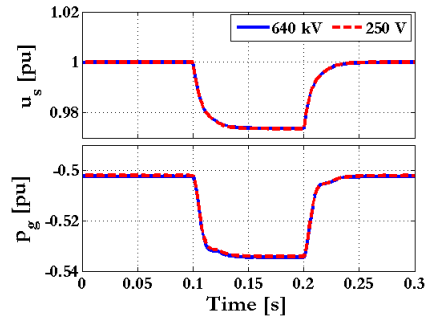

Fig. 4. Validation of the VSC scaling methodology

[20]. Therefore, the DC cable is emulated by a laboratory-scale coaxial cable, to have a similar propagation time as a corresponding high voltage cable. The copper section of the core was chosen to achieve a voltage drop smaller than 5 % per cable for a current of 10 A and a nominal voltage of 250 V. Nexans has proposed using cables with copper sections of 10 mm^2 and 25 mm^2 which leads to a maximal length of 2 km and 5 km, to stay within the voltage bounds. As these cables must be installed in a limited space and for economic reasons, their total length has been limited to 15 km (i.e. 7.5 per pole).

It is known that the first resonance in the classical Π model appears at a lower frequency than the Wide-band Model [21]. The Highest frequency limit of model validity is 20 Hz, too narrow a band compared with the current loop dynamics. To overcome this problem, a little more sophisticated model is introduced. The new model takes into account the coupling between the core and the screen Fig. 5.

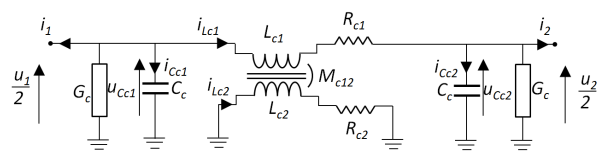
Fig. 5. Positive pole of the Π core-screen coupled model

In the following, the state space model of this special Π section is presented. The pole's differential equations are:

$$\frac{du_{Cc1}}{dt} = \frac{1}{C_{c1}} i_{Cc1} \tag{3}$$

$$\frac{du_{Cc2}}{dt} = \frac{1}{C_{c2}} i_{Cc2} \tag{4}$$

$$\Phi_1 = L_{c1} i_{Lc1} + M_{c12} i_{Lc2} \tag{5}$$

$$\Phi_2 = L_{c2} i_{Lc2} + M_{c21} i_{Lc1} \tag{6}$$

$$u_{Lc1} = \frac{d\Phi_1}{dt} = L_{c1}\frac{di_{Lc1}}{dt} + M_{c12}\frac{di_{Lc2}}{dt} \tag{7}$$

$$u_{Lc2} = \frac{d\Phi_2}{dt} = L_{c2}\frac{di_{Lc2}}{dt} + M_{c21}\frac{di_{Lc1}}{dt} \tag{8}$$

We can obtain a four-order system which represents the pair of cables by arranging these equations.

The cables used to represent the DC grid are a laboratory scale technology of the actual DC cables. The cables are kept on their cable drums to increase their linear inductance and boost the propagation speed Fig. 6. In this configuration, the linear inductance for each line has been measured, and the propagation speed has been calculated. Table II summarizes the actual high voltage DC cable (left value) and the test-bed DC cable (right value) characteristics.

The theoretical wave speed through a coaxial cable is given by the well-known formula:

$$\sigma = \frac{1}{\sqrt{LC}} \tag{9}$$

TABLE II
HIGH VOLTAGE(LEFT VALUE) AND TEST-BED (RIGHT VALUE) DC CABLE CHARACTERISTICS

Link	Cable section $[mm^2]$	Total Cable length $[km]$	Total resistance $[\Omega]$	Total inductance $[mH]$	Total capacitance $[\mu F]$	Propagation time $[\mu s]$
A	$1.54\,10^4$ / 25	25 / 0.45	0.38 / 0.43	2.40 / 17.3	6.79 / 0.19	126.4 / 57
B		50 / 1.14	0.76 / 1.01	4.70 / 43.1	1.35 / 0.47	252.8 / 142
C		75 / 1.82	1.13 / 1.46	7.10 / 69.0	2.04 / 0.74	379.2 / 228
D		100 / 2.27	1.15 / 1.77	9.40 / 86.3	2.71 / 0.93	505.6 / 285
E	$1.54\,10^4$ / 10	100 / 1.45	1.15 / 2.52	9.40 / 58.7	2.71 / 0.46	505.6 / 570

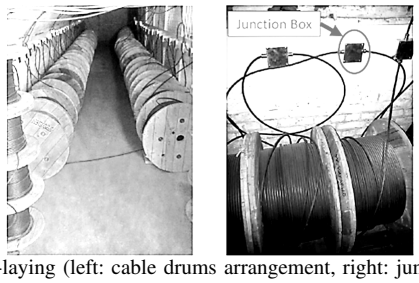

Fig. 6. Cable-laying (left: cable drums arrangement, right: junction between two cables)

B. Test-bed storage and Power flow

Capacitors are key components for the DC grid dynamics; consequently special attention has been paid to have homothetic capacitor values.

TABLE III
IMPLEMENTED STATION CAPACITORS

	Type	Nominal DC Voltage $[V]$	Nominal Power $[W]$	Electrostatic constant $[ms]$	Desired capacitor value $[\mu F]$	Capacitor value $[\mu F]$
GS_1	**Virtual**	250	2200	10	721	721
GS_2	**Physical**		2600		852	1100±20%
WF_1	**Virtual**		2400		786	786
WF_2	**Virtual**		1320		433	440
WF_3	**Physical**		850		279	270±20%

As said above, test-bed converter station capacitors are designed to have the same electrostatic constant as a unitary scale VSC ($i.e.$ around 10 ms) [19]. From the nominal power of converter stations and a 10 ms electrostatic constant, the desired capacitor values are presented in Table III. However, it is not possible to get the exact capacitor values for physical converters (Node 2 and Node 5) since capacitors are sold as normalized values. It should also be pointed out that physical capacitors have a tolerance of 20 %.

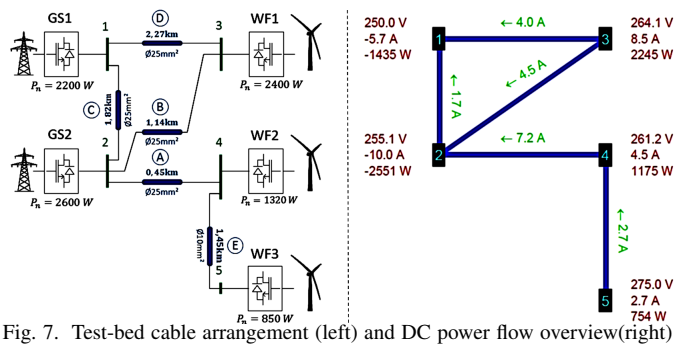

Fig. 7. Test-bed cable arrangement (left) and DC power flow overview(right)

The nominal power of each station has been obtained from a specific scenario performed on the test-bed. It is required that the voltage deviation between the highest voltage level and the lowest voltage level should be below 10 % in normal operations. Thanks to the steady state algorithm and cable data directly measured on the test-bed, a scenario which satisfies the voltage drop requirements has been found. To obtain this scenario, GS_1 has been set at the nominal voltage level (i.e. 250 V), and WF_3 has been set at the highest voltage level (i.e. 275 V). The current through GS_2 has been imposed at 10 A, and currents from WF_1 and WF_2 have been defined at 8.5 A and 4.5 A respectively to get a convenient power flow. The power flow is shown in Fig. 7 (right). This scenario has been considered to define the nominal power of each converter station. The nominal power of each station is sized close to the power flow scenario, apart from GS_1 which is powerful enough to be able to take part of the power currently delivered to the AC grid by GS_2. The nominal apparent power is sized 5 % higher than the nominal real power(Table IV).

TABLE IV
TEST-BED LOAD FLOW AND STATION NOMINAL POWER

	DC Voltage $[V]$	DC Currents $[A]$	Real Power $[W]$	Nominal Real Power $[W]$	Nominal apparent power $[VA]$
GS_1	250	-5.7	-1435	2200	2310
GS_2	255	-10	-2551	2600	2730
WF_1	264	8.5	2245	2400	2520
WF_2	261	4.5	1175	1320	1386
WF_3	275	2.7	754	850	892.5

C. Real time simulated AC system

In order to show how the DC grid can participate in AC ancillary services, converter stations are connected to the AC grid. It has been simulated in real time in the Opal-RT® simulator. In this system, the simulated AC grid deals with hundreds of megawatts while the test-bed deals with thousands of watts. To face this problem, a scale factor is considered between the power extracted from the DC grid

and the one injected into the AC grid. In the simulated AC grid, grid-side converter stations are replaced by power injector sources.

The three wind farms are simulated. It consists of French onshore wind farm profile data, adjusted to the test-bed nominal power constraint and accelerated in time.

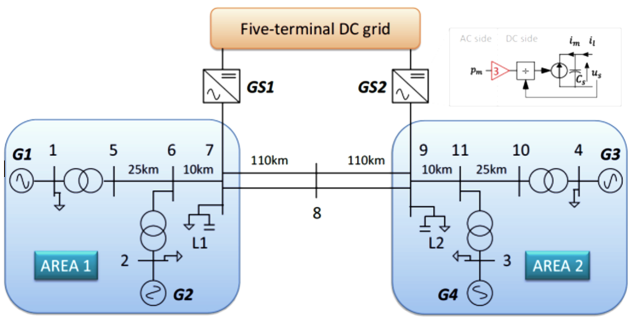

Fig. 8. AC test system connected to test-bed DC through PHIL

The considered AC system, named Kundur grid [16], is presented in Fig. 8. It is a well-known two-area system studied for inter-area oscillations. In this work the AC test system is connected to the five-terminal DC grid, and GS_1 and GS_2 are connected to node 7 and 9 respectively of the AC grid, as shown in Fig. 8.

D. Test-bed supervision based SCADA system and Test-bed signal management

The SCADA system based on PcVue soft is used; it acts as a dispatching center and is able to:

- Monitor quantities of each converter station and states of each component,
- Change the control mode of each converter station,
- Send references to each station's local controller,
- Send suitable converter set points to reach a desired power flow,
- Automatically recalculate converter orders after an event to return to normal operations,
- Monitor and control AC grids,
- Start and stop wind power production,

The test-bed communication scheme is presented in Fig. 9.

The communication between devices is done through an Ethernet network. The communication protocol OPC was chosen to achieve the communication between multivendor devices: PcVue server, Beckhoff PLC, the OPAL-RT® and other client computers. A Beckhoff PLC is embedded in each converter station to be employed as a gateway between a home-made protocol over RS232 serial communication and the OPC over the Ethernet network. The latency of the SCADA system is 1s. Each station receives power and voltage references and returns voltage and current measurements to the SCADA system; Master controller based DC load flow algorithm is implemented in client computers and communicates with SCADA through OPC.

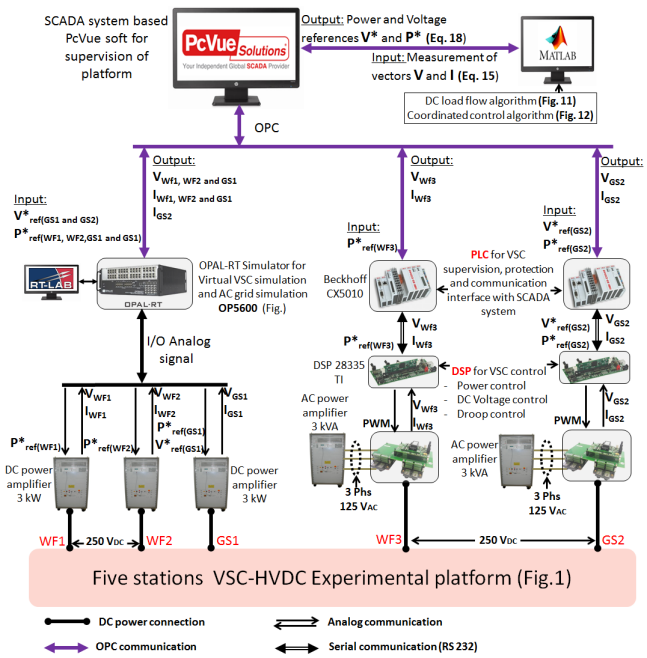

Fig. 9. Test-bed communication scheme

III. Control and Supervision of the Proposed System

A. Assessment of droop control

In this work, a methodology to design the droop value is proposed. It has been seen in simulation that the voltage response time depends on the converter station capacitors, on the droop parameter k and on the number of stations which control the DC voltage m [22], [23]. Moreover, the voltage deviation which comes from a given power deviation is defined by the droop value k and m. The choice of the voltage droop parameter is a trade-off between response time and final voltage deviation. However, the DC voltage control loop is an outer control loop embedding the current control loop. Therefore, system stability is improved when the voltage control loop is slower. Based on this consideration, the droop value was sized to achieve a desired response time. The droop value was chosen with:

$$k = \frac{\tau}{2H_c}\left(\frac{\sum_{j=1}^{m} P_{nj}}{\sum_{j=1}^{n} P_{nj}}\right) \tag{10}$$

Where:

τ	is the time constant of the DC voltage dynamics [s]
H_c	is the DC capacitor electrostatic constant [s]
n	is the number of substation
m	is the number of substation which participates to the voltage control
P_{nj}	is the nominal real power of the jth substation [W]

A test was performed; it focused on DC voltage dynamics when the DC grid is subjected to a severe power change. The objective is to assess the simulation model. To do this, the DC system is first stabilized at an operating point, and then; a fast power reference change is applied at WF_1. For this test, GS_1 and GS_2 are droop controlled with a droop value set at 0.82 pu/pu (calculated from eq. 10 and Table IV). Before the power step change in WF_1, power and DC voltage references of GS_1

are 0.25 pu and 1 pu respectively. The power and DC voltage references for GS_2 are 0.17 pu and 1.02 pu respectively. The power references of WF_1,WF_2 and WF_3 are -0.25 pu, -0.23 pu and -0.27 pu respectively.

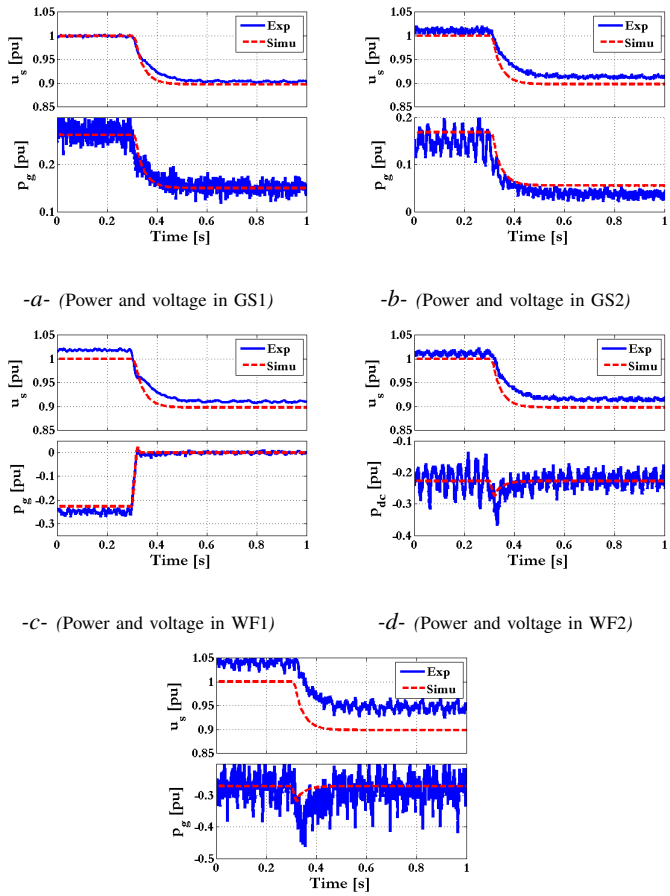

-a- (Power and voltage in GS1)

-b- (Power and voltage in GS2)

-c- (Power and voltage in WF1)

-d- (Power and voltage in WF2)

-e- (Power and voltage in WF3)

Fig. 10. Experimental and simulation results of a step power change of 0.25 pu on WF_1

The scenario is a sudden power reference change from -0.25 pu to 0 pu at WF_1. The change rate of the reference is limited at 13 pu/s. In Fig.10 (a,b,c,d and e) the power and voltage of all converter stations are reported. For GS_1, GS_2 and WF_1 the power is measured on the AC side, while for WF_2 and WF_3, power is measured on the DC side.

The power and voltage are stable before the power variation (before 0.3 s). The power ramp variation on WF_1 is visible in Fig.10-c. In Fig.10-a and Fig.10-b, the power balance is achieved by both grid-side converter stations (GS_1 and GS_2) with similar proportions. Since the power variation leads to a power deficit, the DC voltage level decreases and stabilizes at a lower value. The DC voltage dynamics are around the expected 100 ms response time.

An offline simulation has been carried out with the test-bed parameters and with an equivalent 640 kV MTDC grid using model cable presented in Fig. 5 in order to validate the models. Simulation results are displayed in red dotted lines and compared to experimental results; they are compared in per unit. The dynamics of both voltage and power are very close; the small difference comes from the capacitors of actual converters which cannot be set exactly at the designed value because of the standardized capacitor values. The voltage and power deviations are very similar.

B. Assessment of the coordinated control

For static calculations, the DC grid is only represented by its resistive elements. The studied topology is presented in Fig.11. Conductor cable losses are represented by a series resistance (R_{ij}) and insulation losses by a shunt resistance (R_{ii}).

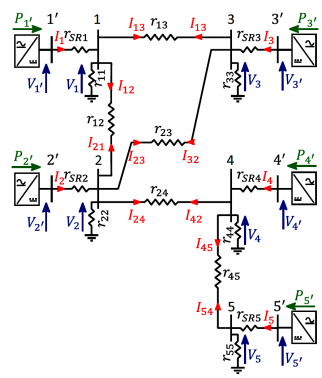

Fig. 11. Static representation of the proposed DC grid topology

The cable conductance is split and equally distributed at the two cable ends. The shunt resistance at each terminal represents the sum of half-conductance of connected cables. In this figure the losses of the smoothing reactor are also taken into account (R_{iSRi}).

At each terminal, the injected current is defined as follows:

$$I_i = \sum_{\substack{j=1 \\ j \neq i}}^{n} \frac{1}{R_{ij}}(V_i - V_j) + \frac{V_i}{R_{ii}} \tag{11}$$

Where

I_i	is the injected current at the ith terminal
V_j	is the voltage at j^{th} terminal
n	is the node number

Considering the whole DC grid, the previous relation can be written in a matrix form:

$$I = Y.V \tag{12}$$

Where

I	is a vector containing injection currents
Y	is the admittance matrix
V	is a vector containing node voltages

The admittance matrix Y can be expressed by:

$$\begin{cases} Y_{ij} = -\frac{1}{R_{ij}} \quad \forall (i \neq j) \\ Y_{ii} = \sum_{k=1}^{n} \frac{1}{R_{ik}} \end{cases} \tag{13}$$

TSOs deal with power instead of currents since they manage energy transfer. Load flow programs are used for this purpose; they solved the following non-linear formula:

$$P = V.I = V.(Y.V) \tag{14}$$

Using the classical load flow algorithm based Newton-Raphson algorithm [24], all power uncertainties are borne by the constant voltage bus. For both primary control and secondary control in the AC system, it seems better to divide this power deviation among more than one converter station. Therefore; a modified Newton-Raphson load flow algorithm is proposed in order to dispatch the power mismatch between several substations, in accordance with the predefined power sharing coefficient called "participation to the coordinated control".

This algorithm has the ability to find a new set of points in order to share the wind power forecast error to several onshore converter stations, to share the power deviation due to unavailability of one converter station and to limit the wind power injection if on-shore converter stations cannot accept more power.

To fulfill this task, a new term related to power deviation is added to the power reference of each station. All converter stations have an initial power reference (P^*), and some of them can adjust their reference to balance the DC grid power flow. The final power delivered by converter stations is given by the following formula:

$$P = P^* + \frac{\alpha}{\sum \alpha} P_{dev} \tag{15}$$

Where:

P	is a vector containing delivered power
P^*	is a vector containing initial power references of all nodes including the constant voltage node
α	is a vector containing the relative participation of each station
P_{dev}	is the power balance error

Unlike the classic method, the power flow of power controlled nodes cannot be guaranteed if their α parameter is not null ($\alpha_i \neq 0$). Depending on the value of α_i, part of the power balance error is allocated to this node. The power balance error is a new unknown which must be solved by a modified load flow algorithm.

When the system operator wants all the wind power harvested to be carried to shore, the power reference vector (P^*) is filled by the actual wind power production (P^*_{WF}) for wind farm converter stations and by the planned power transfer (P^*_{GS}) for grid-side converter stations. The power balance error is shared according to the participation α into the coordinated control. The participation of a given station depends on the participation of other stations, $i.e.$ the higher the α coefficient of a station, the larger the portion of the power deviation taken by this station. The stations which have a null participation parameter act as conventional power nodes. The particular case where there is only one converter which has a non-null α parameter is similar to the previous DC load flow.

The DC load flow must be adapted to take into account the new unknown (P_{dev}). Eq. 16 shows the mismatched power vector:

$$\triangle P^{(k)} = (P^* + \frac{\alpha}{\sum \alpha} P^{(k)}_{dev}) - (V^{(k)}.YV^{(k)}) \tag{16}$$

The correction of the new unknown (ΔP_{dev}) is introduced into the correction vector as follows:

$$\begin{bmatrix} \triangle P^{(k)}_{dev} \\ (\frac{\triangle V}{V})^{(k)}_{(i_{dx\,NV})} \end{bmatrix} = (J^{(k)})^{-1} \triangle P^{(k)} \tag{17}$$

Where

$\triangle P^{(k)}_{dev}$	is the power deviation correction ($0 \leq \mid \triangle P^{(k)}_{dev} \mid \leq \triangle P_{dev\,max}$)
$(i_{dx\,NV})$	is the indexes of not fixed voltage nodes

To solve this linear system, the Jacobian is also modified. Partial derivatives of the first column express the sensitivity of the power deviation on the node mismatched power. They are defined as follows:

$$J_{i1} = \frac{\partial P_i}{\partial P_{dev}} = -\frac{\alpha_i}{\sum \alpha} \tag{18}$$

The flow chart of the load flow is presented in Fig. 12. The inputs of the program are the DC network admittance matrix (Y) , the power reference vector (P^*), the power sharing vector (α) and the initial voltage vector ($V^{(0)}$), while the outputs are the updated voltage vector (V) and the power injection vector (P) .

The scheme of the coordinated control is shown in Fig. 13. The coordinated control calculates new references after a given time ($i.e.$ cyclical operation) or is triggered just after a disruption, such as over-voltage. The TSO preferences are considered. They include the actual wind power production, the power transmission schedule and the desired power deviation sharing. Then, a new load flow is achieved in order to have new set points.

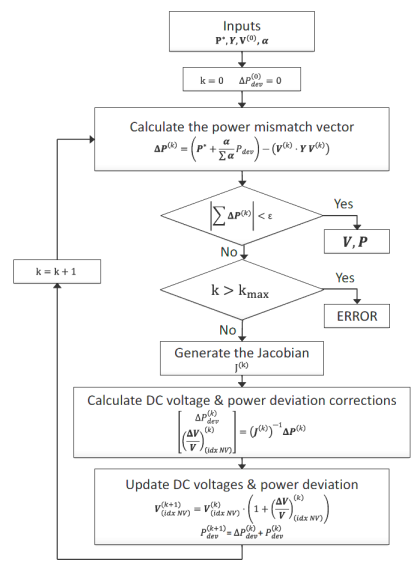

Fig. 12. DC load flow algorithm

1) Normal operation: One day of wind power production is scaled down to the test-bed converter station nominal power. To see the effect if there is no coordinated controller, the same scenario is tested without this controller. For this test, GS_1 and GS_2 are droop controlled with the droop value set at 0.82 pu/pu; the power and voltage references of GS_1 and GS_2 are 0 W / 250 V and 0 W / 250 V respectively.

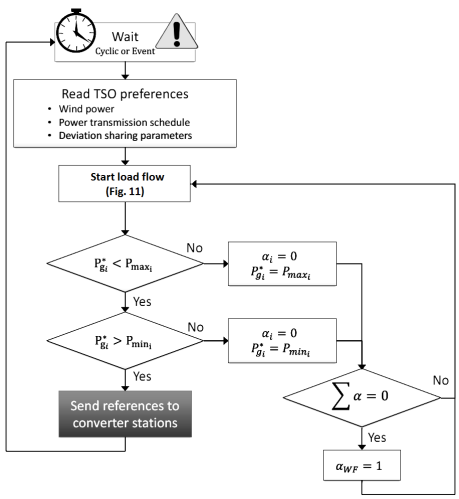

Fig. 13. Coordinated control scheme

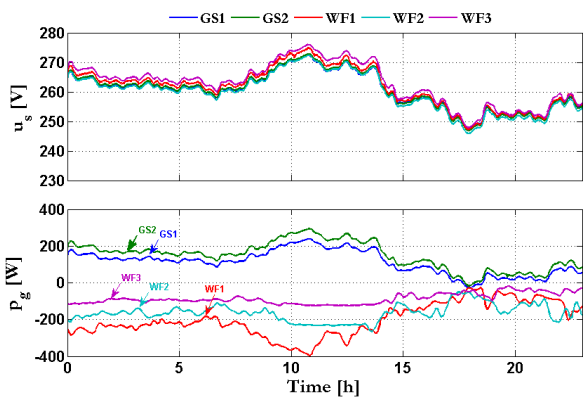

Fig. 14. Experimental results of 1 day of wind power production without coordinated controller

In Fig. 14, the power injected from wind farm stations is shared between GS_1 and GS_2 thanks to the droop control. The power extracted by GS_2 is a bit higher than GS_1 because the nominal power of GS_2 is slightly higher than GS_1. The DC voltage depends on the amount of power injected by the wind farms; the more power there is, the higher the voltage. The DC voltage has already reached 275 V, *i.e.* 10 % over the nominal voltage, even with a power reduced to 20 %.

Now considering a coordinated controller, the converter station references are computed by the Load Flow program with the power sharing capability already presented, which is performed on Matlab® client. The OPC protocol is used for the communication between the SCADA system (PcVue) and Matlab®. The Matlab® client retrieves the information available on the SCADA server about: the actual power production of wind farm converter stations, the desired voltage level for GS_1 set at 250 V and the states of each converter station.

Each 5 s the SCADA system changes a variable to indicate to the Matlab® client that it can start a new load flow. Once the references are calculated, the Matlab® client overwrites the converter set points on the SCADA Server. These set points located on the SCADA server are sent to the converter station each 100 ms; *i.e.* the communication speed between converter stations and the SCADA system.

The Load Flow program has the DC grid admittance matrix, which corresponds to the DC grid topology with measured resistance. To have a similar effect as the droop control that is defined in per unit, the power sharing coefficients of GS_1 and GS_2 are not exactly equal since they do not have the same power rating. The sharing coefficients are:

- GS_1 : $\alpha_{GS_1} = 1$
- GS_2: $\alpha_{GS_2} = 1.18$ $(\alpha_{GS_2} = \alpha_{GS_1} \frac{P_{nGS2}}{P_{nGS1}})$
- WF_1,WF_2 and WF_3 : $\alpha_{WF} = 0$

In Fig. 15, the same wind production profiles are tested with the coordinated controller under the same conditions as for the previous case. Therefore, the new operating points, which are calculated each 5 s, correspond to time steps of 8 min if the production profile time scale is considered. The power profiles of grid-side converter stations are similar to the case without a coordinated controller since power sharing coefficients have been chosen to share power in the same way as for the droop control strategy. The main difference is on the DC voltage map, which is very close to the nominal voltage. Every 8 min the voltage of GS_1 returns to the reference value.

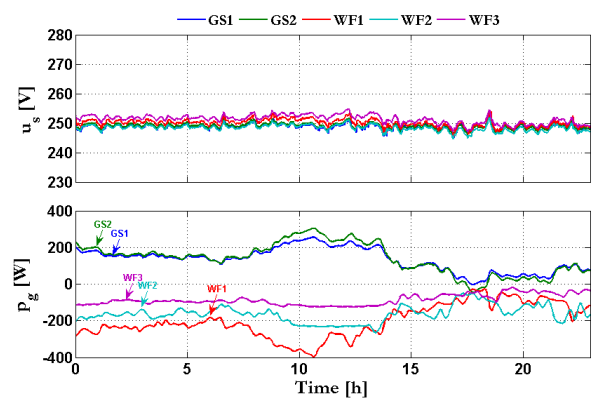

Fig. 15. Experimental results of 1 day of wind power production with coordinated controller

2) Follow-up of the planned grid injection program: The grid-side converter stations can follow a planned AC grid injection program. In Fig. 16, the previous scenario is tested with grid-side power references filled by the injection program ($GS_1^*$and GS_2^*). The DC voltage looks like the previous case; it is still close to the nominal value. In contrast to the previous case, grid-side power transfers attempt to follow the scheduled program instead of just sharing part of the wind power production. It is observed that power through grid-side converters is further from the scheduled program than off-line simulation results. This is due to test-bed losses, notably those of physical converters, which are higher in proportion than for the 640 kV test system and are not considered in the creation of the scheduled injection program. Moreover, it should be noticed that the planned injection program is better followed by GS_1 than by GS_2 since there are more losses in GS_2, which is a physical converter, where as GS_1 is simulated.

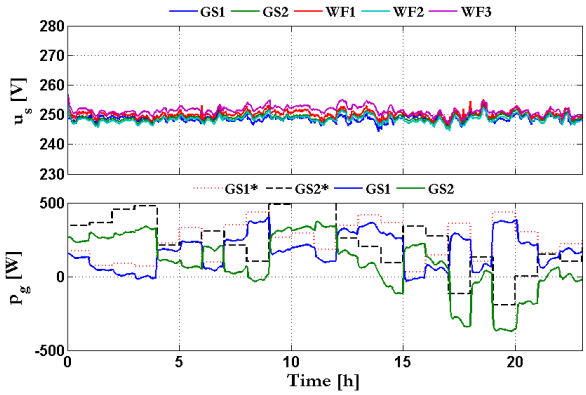

Fig. 16. Experimental results of 1 day of wind power production with coordinated controller using a plan for AC grid side power injection

3) Alleviation of AC congestion: The advantage of the MTDC-HVDC grid is that the DC system can alleviate AC congestion on the AC grid request in real time. To assess this functionality, Kundur's grid [16]is connected to the test-bed grid-side converter. Fig. 17 shows the general structure of the combined AC-DC system where grid side voltage source converter stations are the links between Kundur's grid and the five-terminal DC grid.

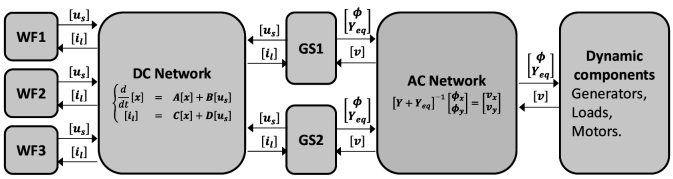

Fig. 17. Block diagram of the AC-DC connected system

The nominal power of GS_1 (resp.GS_2) converter station is 400 MW (resp. 470 MW) on the AC side and 2200 W (resp. 2600 W) on the test-bed. The wind production profiles are the same as in previous cases, however this time an AC grid is connected behind the converter stations. To simulate an overloaded transmission line between the two AC areas, the load located in Area 2 is steeply increased, and in the meantime, the load located in Area 1 is decreased, while generator production is not modified. Once the limit of 300 MW is exceeded between Area 1 and Area 2 (P_{7-9}), the supervisor of the AC system asks the SCADA system to quickly change its grid-side power injections in order to induce a 100 MW decrease on the transmission line. To do so, the SCADA system launches a new load flow to compute new converter station set points with power sharing coefficients for GS_1 and GS_2 (1 and 1.18 respectively); the power references of GS_1 and GS_2 are set at -100 MW(-550 W) and +100 MW(+550 W) respectively.

The DC voltage map is not shown in this figure since it is similar to previous cases with a coordinated controller. Power delivered by GS_1 and GS_2 to the AC system is equivalent to Fig. 15, until the AC system asks the DC system to change its power flows. To alleviate the AC transmission line between the two areas, there is an offset of -550 W (-100 MW) for GS_1 and+550 W (+100 MW) for GS_2, while power injected by wind farm converter stations does not change Fig. 18. This offset leads to a decrease of 100 MW in the power transmitted through the AC line between the two areas.

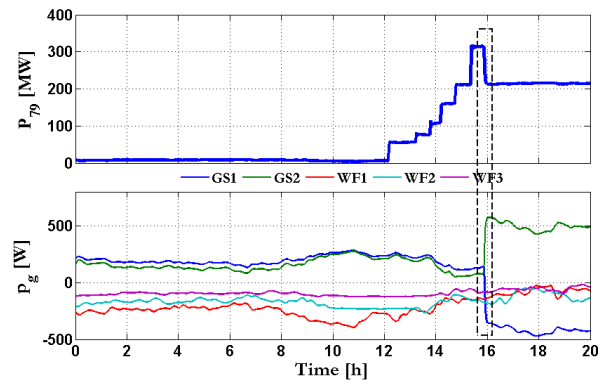

Fig. 18. Experimental results of 1 day of wind power production with coordinated controller- Alleviation of an AC congestion

4) System restoration after a converter outage: It is essential that the coordinated controller can reestablish normal operations after a severe event such as a station tripping. Two tests were carried out to assess this feature; one for an offshore station tripping and another for a grid-side station tripping. For these tests, the primary control strategy is tuned in the same way as in previous cases; grid-side converters are droop controlled, and wind farm converter stations maintain constant power. The coordinated controller updates grid-side converter station references each 5 s, and it is set to share the power harvested by wind farms between GS_1 and GS_2 in relation to their power rating, like for the previous test without the scheduled program. Before computing new set points, the coordinated controller checks if the converter is operating or not. If the converter is not operating, it is not taken into account in the coordinated control.

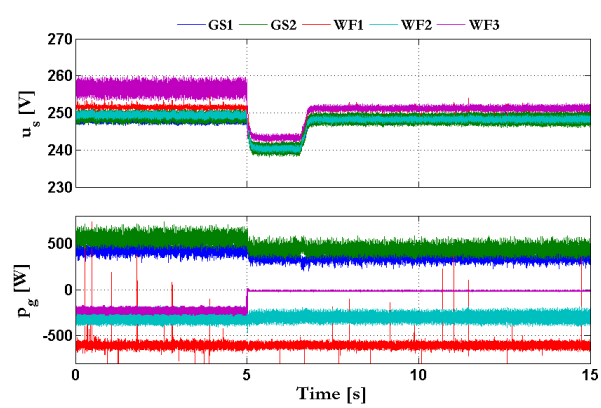

Fig. 19. Outage of a wind farm converter station

In Fig. 19, results of the WF_3 tripping test are shown. At 5 s, the WF_3 is tripped and the power balance is provided by the two grid-side converter stations which are droop controlled. At about 7 s, the coordinated controller sends new power and

voltage references to GS_1 and GS_2. This leads to restoring the DC voltage at nominal value, without any power variation since the power sharing parameters have been set to do the same thing as the droop control power sharing.

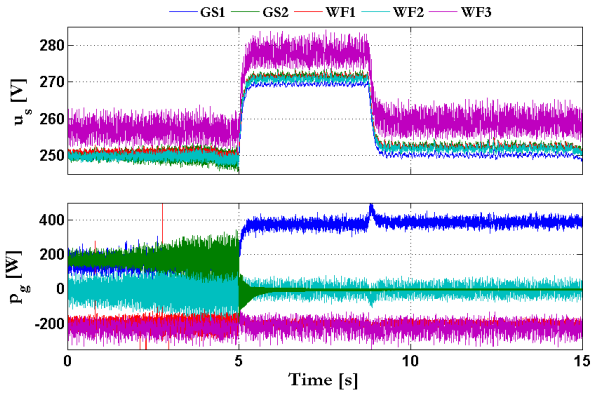

Fig. 20. Outage of a AC grid side converter station

In Fig. 20, results of the GS_2 tripping are displayed. For this test, power injection from wind farms has been decreased again to avoid devastating overvoltage when the GS_2 is tripped. At 5 s, GS_2 is tripped and all the power which was flowing through it is fully reported on GS_1. At around 8 s, the coordinated controller sends new references to GS_1, and therefore the DC voltage goes back to the nominal value, and the power delivered by GS_1 is almost not impacted.

IV. Conclusion

The objective of this work was to develop a laboratory demonstrator with experimental proof to assess offshore DC grid performance. The tests which are carried out on this test-bed are fairly reflective of reality since during the design phase a methodology was set up to have a homothetic laboratory-scale system, and then to represent at best a high voltage grid. The management of the grid is provided by a SCADA system. The demonstrator embeds actual shielded cables which give similar propagation times to actual HVDC cables. Despite excessive voltage drops through cables, the results obtained for droop control on the reduced scale and on the full-scale system exhibit very close dynamics. Also, thanks to a centralized supervisor, it was possible to implement a coordinated control algorithm based on a modified NR algorithm, which is physically independent of the local control. Tests performed with the coordinated controller have shown its effectiveness, either for automatically dispatching power flows or regulating the DC voltage level. As its main contribution, this work has emphasized the DC grid dynamics when it is droop controlled. Also, it has shown the effectiveness of a centralized controller to manage local and independent control without fast communication. On the horizon, the remote control level will be improved to test the behavior in faulty operations. Modular Multilevel Converter (MMC) technology will be integrated instead of classical 2-Level VSC.

References

[1] S. Nguefeu, P. Rault, W. Grieshaber and F. Hassan, “DEMO 3 requirement specifications: detailed specifications for a DC network,” TWENTIES deliverable D11.1. April 2012.

[2] "TWENTIES project," TWENTIES, Final report for EWEA, FP7 Twenties project EC-GA n° 249812, Oct. 2013.

[3] R. Li and X. Wang, "Status and challenges for offshore wind energy," Materials for Renewable Energy & Environment (ICMREE), 2011 International Conference on, Shanghai, 2011, pp. 601-605.

[4] N. Flourentzou, V. G. Agelidis and G. D. Demetriades, "VSC-Based HVDC Power Transmission Systems: An Overview," in IEEE Transactions on Power Electronics, vol. 24, no. 3, pp. 592-602, March 2009.

[5] J. Beerten, O. Gomis-Bellmunt, X. Guillaud, J. Rimez, A. van der Meer and D. Van Hertem, "Modeling and control of HVDC grids: A key challenge for the future power system," Power Systems Computation Conference (PSCC), 2014, Wroclaw, 2014, pp. 1-21.

[6] S. Shah, R. Hassan and J. Sun, "HVDC transmission system architectures and control - A review," Control and Modeling for Power Electronics (COMPEL), 2013 IEEE 14th Workshop on, Salt Lake City, UT, 2013, pp. 1-8.

[7] Q. Fu, W. Du, J. Cao and H. F. Wang, "VSC-based HVDC power transmission for the large-scale offshore wind power — A survey," International Conference on Renewable Power Generation (RPG 2015), Beijing, 2015, pp. 1-6.

[8] L. Livermore, J. Liang and J. Ekanayake, "MTDC VSC Technology and its applications for wind power," Universities Power Engineering Conference (UPEC), 2010 45th International, Cardiff, Wales, 2010, pp. 1-6.

[9] L. Xu, L. Yao, and M. Bazargan, "DC grid management of a multi-terminal HVDC transmission system for large offshore wind farms," 2009 Int. Conf. Sustainable Power Generation and Supply SUPERGEN, pp. 1-7.

[10] J. Sau-Bassols; E. Prieto-Araujo; O. Gomis-Bellmunt, "Modelling and control of an interline Current Flow Controller for meshed HVDC grids," IEEE Transactions on Power Delivery , vol.PP, no.99, pp.1-1, December 2015.

[11] N. R. Chaudhuri, R. Majumder, B. Chaudhuri and J. Pan, "Stability Analysis of VSC MTDC Grids Connected to Multimachine AC Systems," IEEE Transactions on Power Delivery, vol. 26, no. 4, pp. 2774-2784, Oct. 2011.

[12] E. Prieto-Araujo, A. Egea-Alvarez, S. Fekriasl and O. Gomis-Bellmunt, "DC Voltage Droop Control Design for Multiterminal HVDC Systems Considering AC and DC Grid Dynamics," IEEE Transactions on Power Delivery, vol. 31, no. 2, pp. 575-585, April 2016.

[13] S. Goyal, G. Ledwich and A. Ghosh, "Power Network in Loop: A Paradigm for Real-Time Simulation and Hardware Testing," in IEEE Transactions on Power Delivery, vol. 25, no. 2, pp. 1083-1092, April 2010.

[14] J. Descloux, B. Raison and J. B. Curis, "Protection strategy for undersea MTDC grids," PowerTech (POWERTECH), 2013 IEEE Grenoble, Grenoble, 2013, pp. 1-6.

[15] M. Yang, D. Xie, H. Zhu and Y. Lou, "Architectures and Control for Multi-terminal DC (MTDC) Distribution Network-A Review," AC and DC Power Transmission, 11th IET International Conference on, Birmingham, 2015, pp. 1-7.

[16] P. Kundur, Power system stability and control. Tata McGraw-Hill Education, 1994.

[17] N. R. Chaudhuri and B. Chaudhuri, "Adaptive Droop Control for Effective Power Sharing in Multi-Terminal DC (MTDC) Grids," IEEE Transactions on Power Systems, vol. 28, no. 1, pp. 21-29, Feb. 2013.

[18] E. Prieto-Araujo, F. D. Bianchi, A. Junyent-Ferre and O. Gomis-Bellmunt, "Methodology for Droop Control Dynamic Analysis of Multiterminal VSC-HVDC Grids for Offshore Wind Farms," in IEEE Transactions on Power Delivery, vol. 26, no. 4, pp. 2476-2485, Oct. 2011.

[19] S-A. Amamra, F. Colas, X. Guillaud, P. Rault and S. Nguefeu, "Laboratory-based test bed of a three terminals DC networks using power hardware in the loop," 2013 Power Electronics and Applications (EPE), 15th European Conference on, Lille, pp. 1-8.

[20] "HVDC Light power cables - Submarine and land power cables," ABB, Technical brochure - HVC 2GM5001-gb 3000, Apr. 2006.

[21] P. Rault, “Dynamic Modeling and Control of Multi Terminal HVDC Grid,” Laboratoire d’électronique et d’électronique de puissance de Lille, Ph.D. dissertation, March 2014.

[22] G. Stamatiou and M. Bongiorno, "A novel decentralized control strategy for MultiTerminal HVDC transmission grids," 2015 IEEE Energy Conversion Congress and Exposition (ECCE), Montreal, QC, pp. 5794-5801.
[23] N. R. Chaudhuri and B. Chaudhuri, "Adaptive Droop Control for Effective Power Sharing in Multi-Terminal DC (MTDC) Grids," IEEE Transactions on Power Systems, vol. 28, pp. 21-29, 2013.
[24] F. Coffele, R. J. Garcia-Valle and E. Acha, "The Inclusion of HVDC Control Modes in a Three-Phase Newton-Raphson Power Flow Algorithm," Power Tech, 2007 IEEE Lausanne, Lausanne, pp. 419-424.